A Dynamic Mixed-Control Model for BOF Metal–Slag–Gas Reactions

JAYASREE BISWAS, SNIGDHA GHOSH, N.B. BALLAL, and SOMNATH BASU

Basic oxygen steelmaking has been the interest of research for several decades due to its complex and fast process dynamics. To predict the evolution of slag–metal composition and temperature, it is important to control the process efficiently. The framework developed by Sarkar *et al.* (Metall Mater Trans B 46:961–976, 2015) is advanced further to estimate the evolution of chemical composition and temperature of molten metal and slag. In this present study, a period of flight is considered for droplets at the early period of blow when stable emulsion has not formed. The size distribution of the droplets is evaluated according to the Rosin–Rammler–Sperling distribution. A coupled mixed-controlled kinetic model is incorporated in order to quantify the extent of reaction at the interface of a single droplet in the emulsion phase. This kinetic model assumes that transport of species in both metal and slag phases are rate controlling. Reaction kinetics of these individual droplets are tracked at each time step throughout its period of residence in the metal–slag–gas emulsion, to predict the evolution of the metal and slag compositions for the entire converter with blowing time. Evolution of the bath temperature is estimated by developing a thermal model. The predictions from the model, when validated with plant trial data, could efficiently simulate the phosphorus and manganese reversal phenomena, along with the early removal of silicon (Cicutti *et al.* in 6th International Conference on Molten Slags, Fluxes and Salts, Stockholm-Helsinki, 2000, Paper 367, pp. 1–9, 2000).

I. INTRODUCTION

THE basic oxygen furnace (BOF) has firmly established itself as the dominant process of primary steelmaking across geographies and accounted for more than 70 pct of global steel production during 2019 to 2020.[1] BOF steelmaking is a complex process marked by fast reaction kinetics, intense stirring, presence of multiple phases, and strongly exothermic reactions. Since in-blow information is scarce, researchers over the past several decades have attempted to model the reaction kinetics in order to simulate the evolution of slag and metal compositions during the refining to develop a better understanding of the process.

The fast reaction kinetics in the BOF can be attributed primarily to enhance metal–slag, gas–metal, and slag–gas interfacial area, arising from generation of small droplets during the impingement of supersonic jets of oxygen into the metal bath and formation of a metal–slag–gas emulsion.[2] The individual metal droplets in the emulsion are "refined" by oxidation of the solute elements. After a finite residence time, these droplets fall back into the bulk metal bath, which causes overall refinement of the bath. The rate of refining of the dispersed droplet depends mainly upon three factors, *viz.* total population of droplets in the emulsion, size distribution of droplets, and residence time of individual drops. Together, these determine the time and interfacial area available for the chemical reaction(s) of droplets within the slag.

Several experimental studies have been performed to understand the kinetics of decarburization[3–5] and dephosphorization behavior.[6–10] The reaction kinetics have been modeled for a single droplet as well as in a global sense. Sun[11] has modeled the decarburization and desiliconization behavior of an iron droplet with FeO-containing slag, considering the effect of droplet

JAYASREE BISWAS is with the Department of Materials Science & Engineering, McMaster University, Hamilton, ON L8S 4L8, Canada and also with the Department of Metallurgical Engineering & Materials Science, Indian Institute of Technology Bombay, Mumbai 400076, India. Contact e-mail: jayasreebiswas09@gmail.com SNIGDHA GHOSH is with the Department of Fuel, Minerals and Materials Engineering, Indian Institute of Technology (ISM) Dhanbad, Dhanbad, Jharkhand 826004, India and also with the Department of Metallurgical Engineering & Materials Science, Indian Institute of Technology Bombay; N.B. BALLAL and SOMNATH BASU are with the Department of Metallurgical Engineering & Materials Science, Indian Institute of Technology Bombay.

swelling. Although the author presented a qualitative validation of the model, a quantitative validation was absent in the article.

Several static models, based on heat and mass balances, have been developed to provide an understanding of the overall kinetics in the steelmaking process.[12–14] These models are quite widely used by BOF operators to estimate the quantities of flux, coolant, and oxygen addition, necessary for a given set of input conditions, in order to achieve the desired temperature and composition of the steel at the end of the refining process. These models are fairly capable of estimating the overall material consumption but cannot provide an estimate of how the bath temperature and chemical composition varies with time during refining.

Several researchers (Deo et al.,[15] Knoop et al.,[16] Kattenbelt and Roffel,[17] Pahlevani et al.,[18] Shukla et al.,[19] Dogan et al.[20–22]) have attempted to overcome this by incorporating some of the process variables and developing "dynamic" models that aim to simulate various transient phenomena. Deo et al.[15] developed a multicomponent mixed-controlled model to predict decarburization, desiliconization, and demanganization kinetics combining with online measurement of off gas composition and temperature. The model was able to predict the decarburization behavior closely at the initial blow period but deviated largely from the plant data towards the end of the blow. The model was also less effective in capturing the reversion of manganese. Later Knoop et al.[16] extended the multicomponent model developed by Deo et al.[15] by incorporating the droplet generation rate, size distribution, dissolution kinetics of lime, and scrap but with an assumption of constant the residence time. The multicomponent mixed-controlled model by Deo et al.[15] was further utilized by Graveland et al.[23] to simulate the process performance for a variety of operating conditions, such as retained slag and increased addition of calcined dolomite. A few years later, Kattenbelt and Roffel[17] developed a dynamic model by focusing on decarburization, assuming the process to be chemical reaction rate-controlled. They introduced an empirically fitted equation to capture the effect on changing oxygen flow rate and lance height. To simulate the basic oxygen steelmaking process, it was necessary to introduce submodels to individually address the different aspects such as droplet generation, size distribution of droplets, and residence time of droplets in the emulsion. Thus, although the model by Kattenbelt and Roffel[17] predicted well for the specific cases considered, it did not cover the overall dynamics. Pahlevani et al.[18] proposed a coupled reaction model for steel refining, considering the effect of solid phases in the slag. However, this model did not provide any explanation of the multizone reaction kinetics. The model proposed by Shukla et al.[19] took thermodynamic equilibrium into consideration to predict the composition evolution. However, the kinetic aspect was not considered with due rigor. Dogan et al.[20–22] developed a comprehensive model for the BOF process based on multiple zones, incorporating the surface tension effect on droplet generation rate, flux dissolution, scrap melting, and decarburization kinetics. The model was

quite satisfactory, but the authors focused mainly on decarburization kinetics, even though the predicted decarburization rate deviated significantly towards the end of the blow. Lytvynyuk et al.[24,25] proposed a dynamic model of basic oxygen steelmaking based on the coupled reaction model approach for slag metal reactions, included the dissolution behavior calcined lime and dolomite, as well as scrap melting kinetics. This model was able to predict the composition evolution quite satisfactorily but with an assumption of single reaction zone. Based on the model of Dogan et al.,[20–22] Rout et al. recently integrated desiliconization reaction kinetics in the BOF based on multizone reaction approach and predicted the contribution from three different zones as gas–metal, slag–bulk metal and slag–metal–gas emulsion.[26] The study proposed desiliconization reaction(s) to be happening primarily in the slag–metal emulsion zone. However, an ambiguity remains in their approach since emulsion formation is insignificant during the early stage of the blow whereas desiliconization of the metal is significant during this period. Rout et al. also incorporated phosphorus[27] and manganese removal kinetics[28] along with an improved decarburization model.[29] Kruskopf and Visuri[30] proposed a mathematical model based on Gibbs' free energy minimization, considering a single reaction zone. The model was able to predict decarburization behavior well but failed to capture desiliconization properly. Recently Kadrolkar and Dogan[31] developed a decarburization model incorporating the effect of bloating and in another work,[32] they have shown that the contribution from oxygen impact and slag metal bulk reaction zones in overall refining is negligible. Based on the framework developed by Dogan et al.,[21] Dering et al.[33] proposed a first-principle based model to perform dynamic optimization and was able to simulate the temperature evolution and end point carbon concentration well but the silicon removal kinetics were not agreeing. Recently, several researchers[34–38] have developed data-driven models using machine learning algorithms such as support vector machine,[35] support vector regression,[37] principal component analysis with back propagation neural network,[36] adaptive network-based fuzzy inference system along with robust relevance vector machine[34] and predicted the amount of coolant and oxygen required,[34] the end point carbon concentration and temperature,[34,35,37] decarburization rate[38] and the end point phosphorus[36] as well. BOF process dynamics has recently been reviewed by Ghosh et al.[39] as well as Vos et al.[40] and the scope of further improvements has been highlighted.

Despite several attempts to capture the BOF process dynamics in physics-based as well as data-driven models, there is a lack of understanding in the early period of the blow, during which large fraction of the silicon is removed from the metal bath and huge amount of heat is generated. It is important to capture the kinetics of refining reactions in three multiple zones, most importantly in emulsion zone, along with the generation of droplet having a size distribution and temperature evolution of the bath, which are crucial in controlling the reaction kinetics. Some of the current authors, along

with their coworkers, proposed a dynamic model on the basis of Gibbs free energy minimization technique, considering multizone reaction kinetics.[41] Although that model depicted the decarburization profile quite satisfactorily, temporal profiles of other solute elements did not show good agreement with in-plant measurements. The model had limitations in simulating the reversion of manganese, phosphorous, and early removal of silicon and was computationally very intensive as well. Further, features like droplet size distribution and temperature evolution were excluded from the earlier model.

Based on the framework developed by Sarkar et al.,[41] further development[42,43] has been made in course of the present work to address the oxidation and reversion of elements like silicon, phosphorus, and manganese in a more accurate way. An attempt to capture the early removal kinetics of silicon is presented. Dynamic parameters such as evolution of bath temperature, droplet size distribution, and residence time of metal droplets in the emulsion were combined with chemical reactions to improve the reliability of estimation. This approach considers a single metal droplet maintaining chemical equilibrium at its interface with molten slag or gas depending upon the blowing conditions, subject to the kinetic constraints of mass transfer in metal and slag. The single-droplet approach is then applied to each of the resulting droplets in order to estimate the overall composition variation and has been validated with industrial converter data.[44,45]

II. MODEL FORMULATION

The fundamental structure of the model developed in the present work is partly similar to that proposed earlier by Sarkar et al.[41] However, the framework has been expanded to incorporate the chemical reactions involving phosphorus and manganese. The BOF has been visualized as an assemblage of three idealized constant stirred-tank reactors (CSTR), having continuous heat and mass transfer between one another.

Reactor I—Lower part of the metal bath. Relatively less stirred; location of scrap dissolution.

Reactor II—Upper part of the metal bath, containing the hot spot. This reactor shares the interface with slag–metal–gas emulsion.

Reactor III—Slag–metal–gas emulsion zone. Majority of chemical reactions (e.g., oxidation of C, Si, Mn, P) and lime dissolution take place here.

Mixing takes place between the upper and lower portions of the metal bath (Reactors I and II) at a finite exchange rate. When oxygen jet strikes the top of the upper metal bath (Reactor II), all the oxygen is assumed to react with a near-surface layer of molten metal and the oxide products are transferred to Reactor III. Metal droplets generated from Reactor II due to jet momentum are transferred to the emulsion zone (Reactor III). Each droplet falls back to Reactor II after its respective residence time in the emulsion; solute concentration in the metal bath is thus reduced by progressive dilution.

Within a single time step (Δt), the following sequences of calculations are carried out in the 'global' model:

a. Droplets are generated with a distribution of sizes and are transferred to Reactor III. The drops generated at each time step are divided into several size ranges, conceptually identified as a "box." A "box" is identified by the size range and its time of birth (therefore, starting composition).

b. At any point in time, the emulsion contains "boxes" of different age (therefore, of different compositions) and size intervals. The rates of reactions with droplets in each box are determined by the box identity (composition and size) as well as the gas and slag condition prevailing at that instant.

c. During the first two minutes of blow, when the emulsion has not formed, the droplets perform a projectile motion through the gas instead of remaining suspended in the emulsion. The residence time of individual droplets is decided by its trajectory. The rate of refining reactions at the gas/metal interface is assumed to be controlled by mass transport in the metal phase and the interfacial concentrations are estimated from the thermodynamic equilibrium assuming pure oxides are forming. The partial pressure of oxygen in the gas was approximated as that in air.

d. Beyond the first two minutes of reaction, the emulsion is assumed to have formed and the droplets are considered to react with the slag. All the reactions are assumed to be at equilibrium at the drop/slag interface and the rates are determined by mass transfer both in the slag and the metal drop throughout the entire period. The droplets are believed to remain suspended in the emulsion due to emerging CO bubbles until the carbon concentration decreases below a critical level (assumed as 0.2 mass pct in this work), and then those fall down to the bulk metal bath. The terminal velocity of the descending droplets is decided by diameter and viscosity of the surrounding slag/emulsion.

e. Beyond the first two minutes of blowing, the reaction at the interface between slag and bulk metal phases has also been calculated based on assumption that the reaction is slag phase mass transfer controlled.

f. Once the droplets fall back, mixing takes place with the bulk metal and mass balance determines the change in composition of Reactors I and II.

g. Scrap dissolution and lime dissolution take place linearly, and the temperature of the metal bath and slag changes according to enthalpy balance.

III. GOVERNING EQUATIONS

A. Droplet Size Distribution

Several researchers have carried out experiments with the aim to investigate the droplet generation behavior and the influence of changing the lance height.[46–48] Subagyo et al.[49] proposed an empirical correlation of droplet generation rate as a function of a blowing number ($N_B =$

$\rho_g u_g^2 / 2\sqrt{\sigma g \rho_M}$) which is employed in this model. The gas velocity (u_g (m/s)) varies linearly with the axial gas velocity which has been evaluated as a function of lance height and oxygen jet velocity at the point of nozzle exit from the correlation developed by He and Standish.[50] A detailed investigation was carried out by Koria and Lange[51] on the droplet size distribution . Considering dynamic and geometric similarity, they showed that droplet size distribution could be approximated by the Rosin–Rammler–Sperling function[52]

$$R = 100 \exp\left(-\left(\frac{d}{d'}\right)^n\right)\% \qquad [1]$$

where R is the cumulative weight percentage (pct) remaining on the sieve of diameter d, and n and d' are the parameter for distribution and the characteristic diameter (m), respectively. Essentially, d' corresponds to $R = 36.8$ pct. One can define other characteristic diameters by appropriately scaling the cumulative percentage remaining (R). Koria and Lange[51] used limiting droplet size (d_{limit}(m)), which is corresponding to $R = 0.1$ pct as the characteristic diameter of the drops. By non-dimensionalizing Eq. [1] and assuming that $d = \emptyset \cdot d_{limit}$, it can be shown that[51,52]

$$R = 100[(0.001)^{(d/d_{limit})^n}] \qquad [2]$$

The exponent n of this distribution function is found to be independent of blowing parameters and place of collecting the drops whereas d_{limit} is found to be dependent on both. The value of n was reported to be 1.26. On the other hand, d_{limit} was represented as a function of various experimental parameters, as given in Eq. [3]

$$d_{limit} = 5.513 \times 10^{-3}$$
$$\left[\frac{6.91 \times 10^5 \times N \times (d_t^2/x^2) p_a [1.27(p_0/p_a) - 1] \cos\theta}{N}\right]^{1.206}$$
$$[3]$$

where p_0 is the nozzle exit pressure (Pa), p_a is the ambient pressure (Pa), N is the number of nozzles in the lance, θ is angle (deg) of inclination of each nozzle relative to lance axis, d_t is throat diameter (m) of nozzle, and x is the dynamic lance height (m). This correlation allowed estimation of the cumulative weight distribution of droplets across the entire size range.

The residence time(s) of the droplets of different sizes was earlier studied by several workers[51,53,54] who put forth correlations to estimate the terminal velocity of the droplets. The model proposed earlier by Sarkar et al.[41] was based on residence time estimation using the correlation by Subagyo et al.[53] The same correlation is adopted in this current work to estimate the residence time of individual droplets.

B. Activities in Molten Metal and Slag

The activity coefficients of metalloids and slag components are calculated depending on the metal compositions and the slag compositions, respectively. The activities of the metalloids are calculated on the basis of Henrian 1 wt pct solution in iron using interaction parameters reported by Sigworth and Elliot.[55] The activities of the oxides are defined as $a_i = \gamma_i X_i$, where a_i, γ_i, and X_i are the activity, activity coefficient[56–59], and the mole fraction of oxide i, respectively.

The activity coefficient of SiO_2 is derived by curve fitting the data of thermodynamic activity published in Slag Atlas[56] for the CaO-FeO-SiO_2 system, under the condition of lime saturation. Regular solution approximation has been adopted to account for temperature dependence of $\gamma(SiO_2)$.

$$T \ln \gamma_{SiO_2}^b = -1176.7 - 7427.6 \times \frac{X_{FeO}}{X_{SiO_2}}$$
$$+ 1662.2 \left(\frac{X_{FeO}}{X_{SiO_2}}\right)^2$$
$$\text{if } \frac{X_{FeO}}{X_{SiO_2}} < 1$$

$$\gamma_{SiO_2}^b = 0.005 \quad \text{if } \frac{X_{FeO}}{X_{SiO_2}} \geq 1 \qquad [4]$$

The activity coefficient of MnO was evaluated using a correlation based on the variation of $\gamma(MnO)$, as a function of slag basicity, reported by Turkdogan and Fruehan.[57]

$$\gamma_{MnO}^b = \begin{bmatrix} -0.07 \times B^3 + 1.012 \times B^2 - 5.026 \times B + 9.853 & \text{if } B > 2.239 \\ 0.569 \times B^3 - 1.176 \times B^2 + 0.979 \times B + 0.123 & \text{if } B \leq 2.239 \end{bmatrix}$$
$$[5]$$

where B = wt pct CaO/wt pct SiO_2. The activity coefficients of FeO and P_2O_5 were estimated using correlations proposed by Basu et al.[58,59]

$$\log \gamma_{FeO}^b = \frac{1262}{T} - 1.1302 X_{FeO} + 0.96 X_{SiO_2} + 0.123 X_{CaO}$$
$$- 0.4198$$
$$[6]$$

$$\log \gamma_{P_2O_{5(l)}}^b = -6.775 X_{CaO} + 2.816 X_{MgO} - 4.995 X_{FeO}$$
$$+ 1.377 X_{SiO_2} + \frac{1007}{T} - 13.992$$
$$[7]$$

In the above Eqs. [4] through [7], pure crystoballite, liquid MnO, liquid FeO, and liquid P_2O_5 were considered as the standard state for SiO_2, MnO, FeO, and P_2O_5, respectively.

IV. REACTION MODELING OF DROPLETS

A. *Flight Model*

During the initial period when enough slag has not been generated to form emulsion and lime has not dissolved, the generated metal droplets follow a projectile motion in the gas phase and react with the oxidizing gas. The remaining oxygen reacts with the metal bath completely oxidizing a layer. The reactions of a single droplet in the 'flight model' are assumed to take place in the thermodynamic order of Si > Mn > C and are metal-side mass transfer controlled. The contribution from metalloid removal reactions of an individual metal droplet with oxidizing gas is summed for all the different sized droplets to calculate the total contribution in refining during the 'flight' period. The mass transfer coefficients (k_M^m (m/s)) of metalloids are estimated using Higbie's Penetration theory[60] as

$$k_M^m = \frac{2}{\pi}\sqrt{\frac{D_i v}{r}} \quad [8]$$

where D_i is the diffusivity (m²/s) of the element at that temperature, v is the surface velocity (m/s), and r is the radius (m) of the droplet. Surface velocity was assumed to be same as that of the droplet velocity. The droplet temperature is assumed to be evolving linearly with time during this period.

The residence time (seconds) of the droplets in the gaseous phase (time of flight) is estimated on the basis of the ejection velocity and the projectile trajectory:

$$t_{\text{flight}} = \frac{2u_0 \sin\theta_0}{g} \quad [9]$$

where u_0 is the ejection velocity (m/s) and $\sin\theta_0$ is the ejection angle (deg). It has been assumed that the ejection angle and ejection velocity, for a given lance and nozzle geometry, remain constant throughout the period of flying and do not depend on the droplet size. The jet momentum, which determines the ejection velocity and ejection angle of droplets from metal bath, is dependent upon the lance height and nozzle geometry. Hence, the current assumption is fairly reasonable.

B. *Droplet Reaction in Emulsion*

When a metal droplet is ejected into an environment of oxidizing slag, the metalloids start to oxidize from the drop simultaneously. A schematic is presented in Figure 1. Here, thermodynamic equilibrium is supposed to prevail at the slag/metal interface, with mass transfer in the slag and metal controlling the rate. The mass transfer coefficients of the metalloids were estimated using Higbie's Penetration theory, Eq. [8], with the relative velocity between the droplets and the metal being the corresponding terminal velocity.[60]

For an elemental reaction taking place at the slag metal interface of the droplet

$$m[M] + n[O] = (M_mO_n)$$

Thermodynamic equilibrium can be expressed according to the following equation –

$$K_{M_mO_n} = \frac{X_{M_mO_n}^i \gamma_{M_mO_n}^b}{([\text{pct M}]^i f_M^b)^m ([\text{pct O}]^i f_O^b)^n} \quad [10]$$

where M is the element, *e.g.*, C, Mn, Si, and P. Fe is essentially the solvent species in the molten metal and is assumed to behave ideally; Eq. [10] has been modified accordingly. For the various solute species, f_M^b is calculated considering the interaction up to second order with interaction parameters reported by Sigworth and Elliot.[55]

The mass transfer rates in metal and slag are matched according to the following equation –

$$\frac{k_M^m \rho_M \left([\text{pct M}]^b - [\text{pct M}]^i\right)}{\text{Molar Wt of M}}$$
$$= \frac{k_{\text{slag}}\rho_{\text{slag}}\left([\text{pct M}_mO_n]^i - [\text{pct M}_mO_n]^b\right)}{\text{Molar Wt of M}_mO_n} \quad [11]$$

Equation [11] is valid for Mn, Si, and P. Here, the activity coefficients of slag and metal components have been estimated as per the bulk composition. The main purpose of adopting this approximation was lower computation time.

The numbers of moles of oxygen required (N_O) to transfer of the metalloids (Si, Mn, P, and Fe) are

$$N_o^{M_mO_n} = n\Delta t \rho_{\text{slag}} A k_{\text{slag}} \frac{[\text{pct M}_mO_n]_i - [\text{pct M}_mO_n]_b}{100 \times \text{Molar Wt of M}_mO_n} \quad [12]$$

To consider the CO/CO_2 equilibrium at that temperature, O moles required for C are written as-

$$N_o^{CO/CO_2} = \Delta t \rho_{\text{steel}} A k_C \frac{[\text{pct C}]_b - [\text{pct C}]_i}{1200}(2 - X_{CO}) \quad [13]$$

The oxygen concentration difference between the bulk of the droplet and the slag–metal interface would drive diffusional mass transfer of oxygen inside the droplet. The moles of O thus transported can be calculated by

$$N_o^{\text{Diffusion}} = \Delta t \rho_{\text{steel}} A k_O \frac{[\text{pct O}]_b - [\text{pct O}]_i}{1600} \quad [14]$$
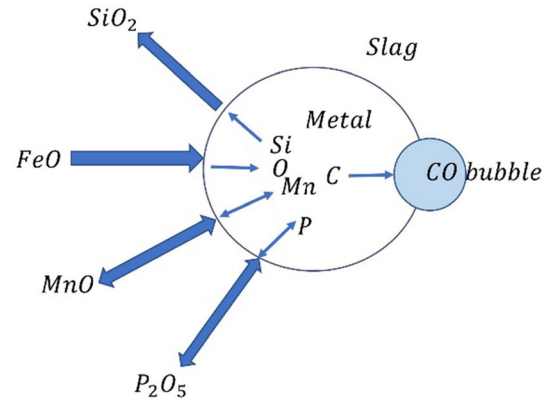

Fig. 1—Schematic diagram of the transfer of metal and slag.

Once chemical equilibrium is achieved and steady state is established, the moles of oxygen transferred from FeO should be equal to the total moles of oxygen consumed for oxidation of C, Si, Mn, and P, as shown in the following relation –

$$N_O \text{ for FeO} = -N_o^{\text{Diffusion}} + \sum_{M=Si,Mn,P} N_o^{M_mO_n} + N_o^{CO/CO_2}$$

[15]

The sets of equations Eqs. [10] through [15] were solved iteratively by bisection method, using MATLAB, and yielded a unique solution. It is to be noted that this simultaneous metalloid removal reactions are occurring at the interface between an individual liquid metal droplet and emulsion and in the similar way, the total refining in emulsion at each time step for all different sized droplets has been calculated by summing the contribution from individual droplets. With the increase in number of droplets in the emulsion, the total slag/metal interfacial area rises, and this huge surface area for reaction fastens the overall bath metal-refining kinetics.

C. Slag–Bulk Metal Reaction

The refining reactions at the interface between slag and bulk metal have also been considered in this work. The interfacial area of reaction has been calculated depending upon the number of nozzles, diameter of the converter, and assuming expansion of supersonic jet at an angle 20 deg after the potential core has ended. The rate of the refining reactions at the slag/bulk metal interface is calculated in the similar way as it is performed for the reaction of a droplet in emulsion. For the slag bulk metal reaction, the mass transfer coefficient of metalloids in metal phase is selected a high value (0.1 m/s) so that the mass transport in the slag phase transport controls the rate of reaction in this zone. It has been assumed that this bulk metal slag reaction occurs only after the initial two minutes of blowing, when the slag has generated enough to cover the bulk metal bath. The contribution in refining from this zone is found to be negligible.

D. Thermal Balance Model

It is important to develop a thermal balance model to predict the evolution of temperature of the slag and the metal bath with blowing time. The thermodynamics and kinetics of the refining reactions are strongly dependent upon the temperature of the individual reactors. In this work, the heat balance was performed for individual reactors at each time step through supply–demand calculations. As no stable emulsion forms in Reactor III during the initial two minutes of the blowing period, a linear rise in temperature was assumed in all three reactors resulting in 50 K rise in temperature due to the vigorous oxidation reactions. Due to inadequate understanding on the initial period, as well as scarcity of measured values, the authors have proceeded with this assumption. The temperature estimation module has been introduced two minutes onwards till the end of the blow.

The main source of heat in the converter is the oxidation reactions in the impingement zone. The oxygen jet (at 300 K) hits the metal bath and generates oxides which go to Reactor III, i.e., the emulsion. The heat generated at the impingement zone was assumed to get distributed among the product oxides and Reactor II (due to the fast conduction of heat) in a ratio of 2:8. With the current assumption, the temperature of the impingement zone is estimated to reach close to 2400 K to 2600 K, based on the oxygen flow rate considered and this is similar to the range reported by Koch et al.[61] as well as Lee et al.[62] Hence, the assumed ratio can be considered as reasonable.

The heat generated in the emulsion due to refining is accounted to Reactor III heat balance. Due to continuous generation of droplets from Reactor II, a transfer of sensible heat is considered from Reactor II to Reactor III. At the same time, when the droplets fall back into Reactor II at the end of refining, it transfers the sensible heat from Reactor III to Reactor II. Additionally, Reactor I and Reactor II continuously exchange heat through mixing. The enthalpies of lime and scrap dissolution are considered in the Reactor III and Reactor I thermal balance, respectively. In addition to that, the loss of heat due to radiation and conduction from the reactor are also incorporated as a fixed percent of the sensible heat throughout the blowing period. It is observed that the foremost contribution of the heat source for Reactor II comes from the heat generated at the impingement zone.

These submodels are incorporated into the 'global' model which simulates the overall slag and metal composition profile of the bath with blowing time.

V. RESULTS

A. Global Model Input Parameters

Simulations have been carried out for a typical BOF blow of 16 minutes. The input parameters are presented in Table I and are similar to the in-plant trials in an industrial BOF reported by Cicutti et al.[44,45]

B. Single Droplet in Emulsion

As outlined in the earlier section, a single-droplet model of 2 g metal droplet reacting in 100 g slag was developed for the droplets in the gas–metal–slag emulsion, based on a coupled mixed-controlled model in which mass transfer in slag and metal phases was limiting the reaction kinetics. Chemical equilibrium was assumed to have been attained at the slag–metal interface. This model was used to estimate the rates of reactions involving individual droplets, for specific slag compositions. The two sets of metal and slag compositions correspond to the initial and the mid-blow period during refining in a BOF are presented in Tables II and III. The results from the single-droplet model for

Input Parameters	Value
Initial Hot Metal Composition and Weight (At Blowing time 2 min)	180,000 kg, wt pct C 3.99, wt pct Si 0.48, wt pct Mn 0.6 wt pct P 0.068
Scrap Composition and Weight	20000 kg, wt pct C 0.05, wt pct Si 0.2, wt pct Mn 0.06 wt pct P 0.015
Initial Slag Composition and Weight	Initial slag weight at 2 min 4275 kg, total lime added 7600 kg, Quartz 800 kg, ore 1900 kg slag composition at 2 min: wt pct FeO 40.5, wt pct MnO 7.32, wt pct SiO_2 21.2, wt pct P_2O_5 0.001, wt pct CaO 26.9, wt pct Al_2O_3 3.73, wt pct MgO 0.35
Hot Metal Temperature (K)	1500 K
Oxygen Blow	620 Nm^3/min, 6 hole nozzle
Bottom Blow (Ar/N_2)	Not considered
Lance Height	2.5, 2.2, 1.8 m
Steel Density	7000 kg/m3
Slag Density	4000 kg/m3
Surface Tension of Steel	$\sigma = [1913 + 0.43 \times (1823 - T) + 67.75 \times [\text{wt pct C}] - 0.107 \times T \times \ln(1 + K_S a_S) - 0.153 \times T \times \ln(1 + K_O a_O)] \times 10^{-3} (\text{N/m})$[63]
Viscosity of Slag	0.0709 Pa s
Mass Transfer coefficient in slag	1×10^{-5} m/s[3]
Diffusion Coefficient in Metal Phase	$D_C = 1.1 \times \left\{1 + \frac{\text{wt pct C}}{5.3}\right\} C \times 10^{-8}$ m^2/s[64] $D_{Mn} = 1.8 \times 10^{-7} \times \exp\left(-\frac{13,000}{RT}\right)$ m^2/s[65] $D_{Si} = 5.1 \times 10^{-7} \times \exp\left(-\frac{9150}{RT}\right)$ m^2/s[65] $D_P = 6 \times 10^{-9}$ m^2/s
Droplet Diameter	1 to 5 mm
Metal Exchange Rate	5000 kg/s[41]
Reactor Ratio	1[41]

Table II. Metal Composition (in Mass Pct) Selected for Single-Droplet Model

Time Period	C	Mn	Si	P	O
Initial Blow	4	0.7	0.45	0.07	0.001
Mid Blow	1.125	0.309	0.0308	0.0359	0.001

simulation of 200 seconds, for two different starting slag and metal compositions, are demonstrated in Figures 2(a) and (b).

It can be observed in Figure 2(a) from the prediction that for the droplet with starting slag and metal composition as that of the initial blow period, a rapid drop of silicon is observed which is followed by removal of carbon and manganese. At the end, phosphorus starts to get oxidized when carbon and manganese concentrations in the droplet have lowered significantly. Whereas in Figure 2(b) for the droplet with starting composition as that of the mid-blow period, phosphorus and manganese start to revert from very early period due to low FeO concentration (~ 9 wt pct) in the slag unlike the earlier case in which FeO concentration in the slag is high (~ 40 wt pct). This substantiates that with proper estimation of activity coefficients in the slag and metal, the single-droplet model is adept to simulate decarburization, desiliconization, as well as reversion of phosphorus and manganese during the mid-blow period due to low oxygen potential of the slag. This single-droplet model was deployed for droplets of each size range that were generated from the Reactor II and underwent refining in the emulsion.

C. Droplet Generation Rate with Lance Height Variation

Figure 3 presents the variation of the lance height with the progress of the blow, and in the same figure, the droplet generation rate variation is also presented. As discussed in the earlier section, with the variation of the lance height, the blowing number changes due to variation in the critical gas velocity (u_g). This figure depicts that with lowering the lance height, droplet generation rate increases, and this is consistent with the observation of other workers.[41,31] The droplet generation rate in the early period (initial two minutes) has been increased by ten times of that rate which is predicted from the correlation developed by Subagyo et al.[49] The correlation by Subagyo et al.[49] was developed for a metal bath with a continuous slag layer at the top. There are experimental[66] as well as CFD studies[67] which illustrates the effect of slag(or upper phase) layer thickness on the droplet generation rate. A tendency to lower the droplet generation rate was observed with increase in slag(or upper phase) layer thickness due to consumption of jet momentum energy by the slag layer and this justifies the modification of the droplet generation rate in the current work at the early period. Further research is needed to understand the droplet generation behavior in this period.

D. Evolution of Overall Metal Composition

Figure 4 illustrates the change in the overall composition of the metal bath with the blow. Small waviness in the curves corresponds the points where the lance height is altered discretely. It is noteworthy that the model could predict in good agreement with the published[44] data quantitatively for oxidation of silicon and carbon,

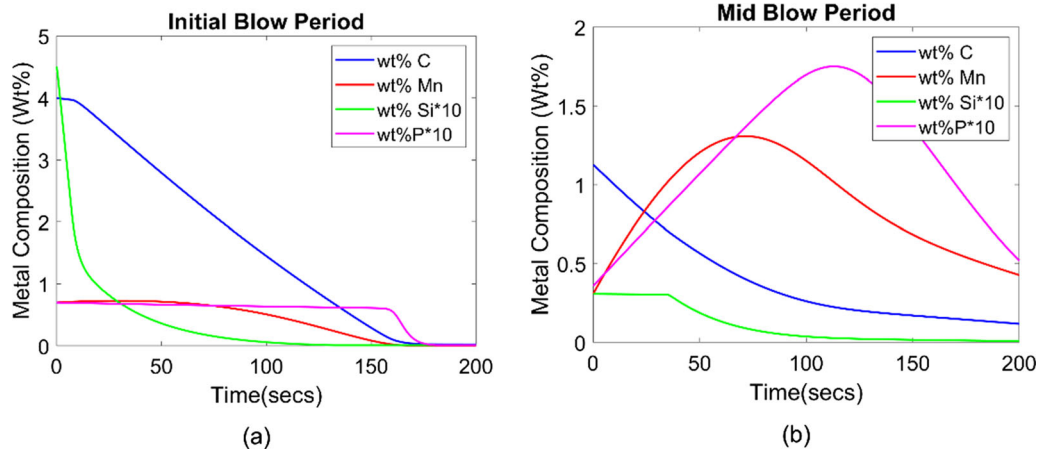| Time Period	FeO	MnO	SiO$_2$	P$_2$O$_5$	CaO	Al$_2$O$_3$	MgO
Initial Blow	39.8	1.2	26	0.001	25	3	5.025
Mid Blow	8.671	7.943	23.251	0.785	52.385	1.702	5.263

Fig. 2—Single-droplet model prediction for (*a*) initial blow period and (*b*) mid-blow period starting composition.
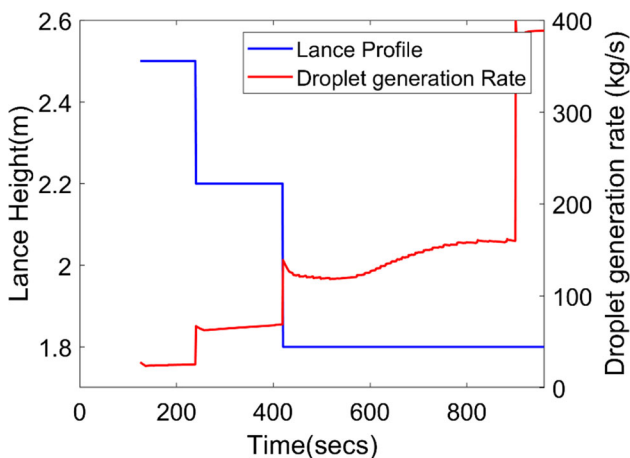

Fig. 3—Droplet generation rate variation with lance height variation.

and qualitatively for phosphorus and manganese. Figure 4(a) depicts the rapid decline of silicon concentration within the initial two minutes of the blow when the droplets are suspended in air and afterwards the rate of removal diminishes, which agrees with the published data.[44,9,68,69] The decarburization rate is very small for a brief period at the beginning of the blow but escalates as soon as silicon and manganese concentrations have reduced substantially. The rate of decarburization is relatively constant during the mid-blow period. It can be noticed that manganese concentration reduces initially when MnO concentration in the slag is low and eventually it starts to revert during the mid-blow period. Phosphorus concentration in the metal decreases sharply as soon as the droplet enters the emulsion phase but reverts partially after 50 to 60 pct of the refining duration, coinciding with low FeO concentration in the slag. Similar trend has been reported by several BOF operators as well as investigators.[44,68,69] In Figure 4, the results from the current model have been compared with the results of Cicutti,[44] with and without considering the Rosin–Rammler–Sperling size distribution. The significant effect of droplet size distribution on the kinetic of phosphorus and manganese oxidation, compared to that of carbon and silicon, is seen very distinctly in Figure 4.

E. Evolution of Slag Composition

Figure 5 shows the evolution of slag composition during the blow. The FeO concentration in the bath increases during the soft blowing period (large lance height) as decarburization rate is less during that time. After that, the FeO concentration decreases to almost 10 pct during the mid-blow period when the droplet generation rate increases; the decarburization rate increases simultaneously. Subsequently, the decarburization rate decreases towards the end of blowing and the FeO concentration in the slag goes up again. Lime dissolves continuously into the slag, which is reflected in the increasing trend of CaO concentration profile for most part of the blow. Towards the very end, sudden rise in FeO concentration dilutes the dissolved CaO in the slag. The percentage of SiO$_2$ in the slag initially increases due to fast oxidation of silicon and subsequently decreases gradually as the overall slag volume slag increases over time. The concentrations of MnO and P$_2$O$_5$ initially increase, then decrease (coinciding with reversion of manganese and phosphorus) and then increase again towards the end-blow.
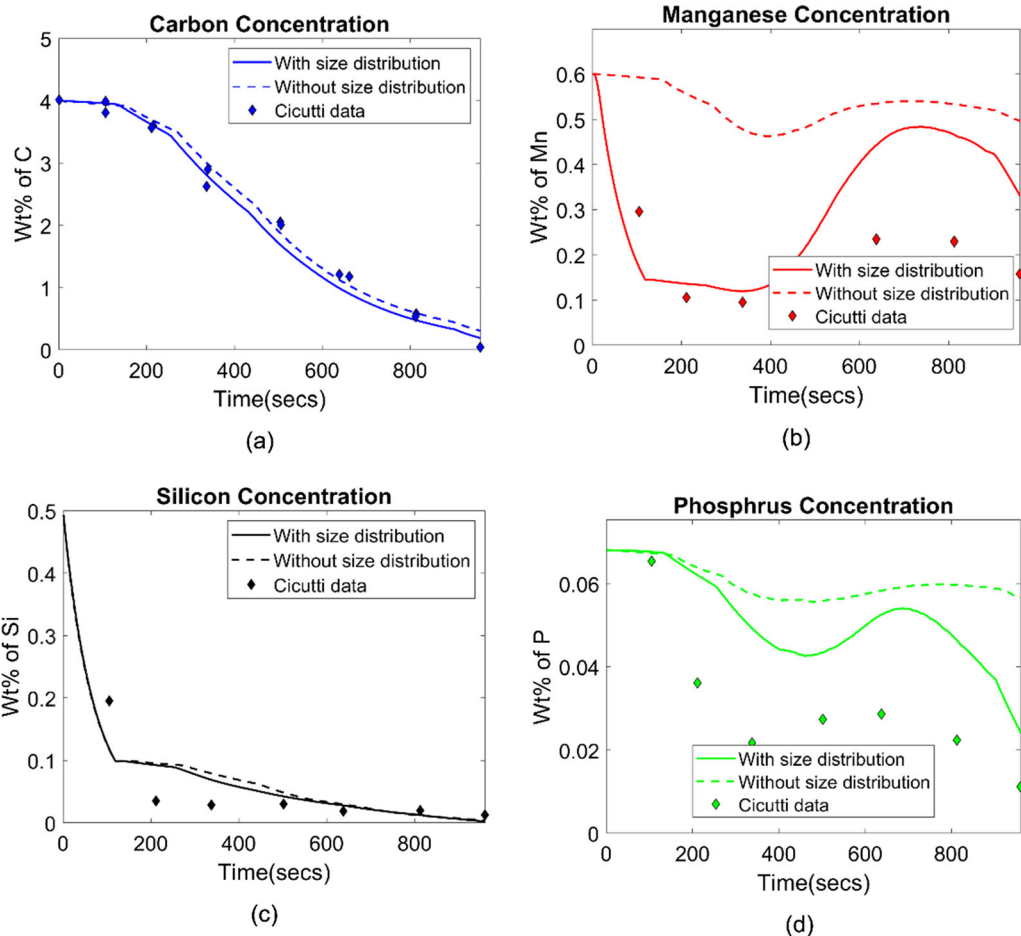
Fig. 4—Change in overall composition of bath metal in weight percentage (pct) during refining (*a*) carbon, (*b*) manganese, (*c*) silicon, (*d*) phosphorous.
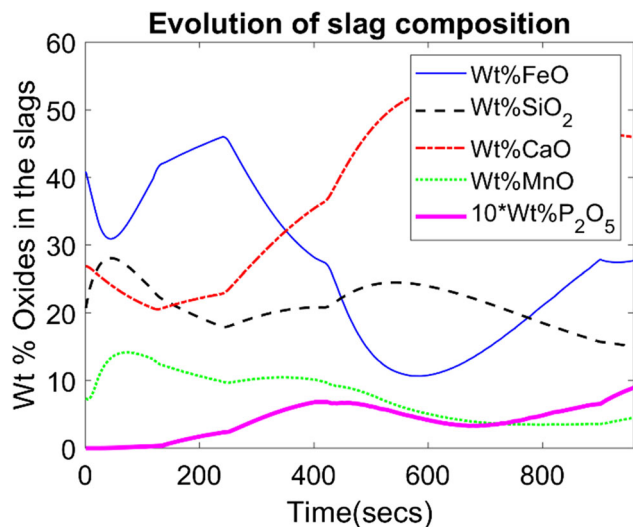

Fig. 5—Slag composition variation in weight percentage (pct) during blowing period.

F. *Variation in Dissolved Oxygen*

Dissolved oxygen concentration in the metal increases with progress of refining as the concentrations of solute elements like C and Si decrease. Figure 6 shows the variation of oxygen and carbon concentrations estimated in the bulk metal during the progress of refining. The oxygen concentration that would have been in equilibrium with the carbon level has also been indicated with the broken line. This evidently shows that while chemical equilibrium is maintained at the metal–slag and metal–gas interfaces, composition of the bulk metal may differ significantly. The highly negative interaction parameter[55] between carbon and oxygen leads to a disproportionately low activity coefficient of oxygen at high carbon concentration (*i.e.,* towards the beginning of the blow). This leads to the apparently anomalous shape of the curve depicting oxygen concentration variation. Figure 7 demonstrates this further by illustrating the mutual variation of carbon and oxygen concentrations.
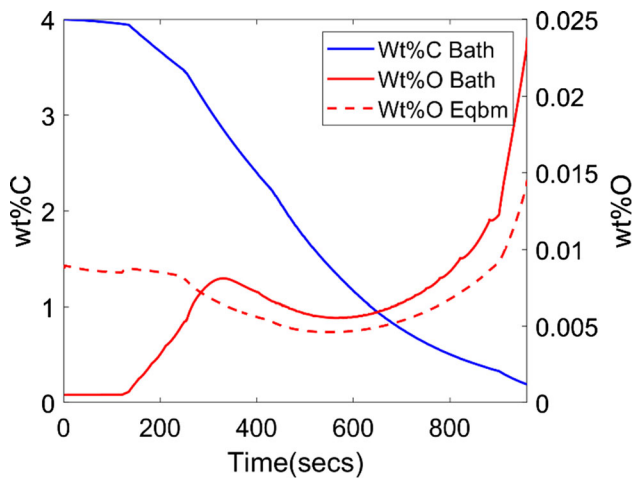
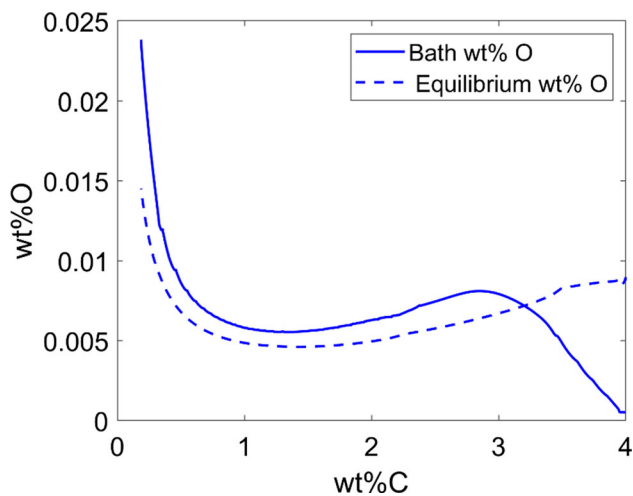Fig. 6—Variation of carbon and oxygen concentrations in weight percentage (pct) with progress of refining.

Fig. 7—Inter-dependence of carbon and oxygen concentrations in weight percentage (pct).

Fig. 8—Temperature variation in bulk metal (Reactors I and II) and slag (Reactor III).

G. Temperature Evolution

Figure 8 shows the temperature variation in the three reactors. It has already been mentioned that a linear increase in temperature was assumed for the first two minutes of the blowing period. Beyond that, the thermal balance model estimates the temperature of the metal bath (both bottom and top) as well as the emulsion, as refining progresses. The figure shows a continuous increase in temperature of both metal and slag with the progress of reactions. Heat is generated continuously due to oxidation reactions in the impingement zone as well as in the emulsion. At the same time, processes like dissociation of oxides and dissolution of scrap and lime add endothermic component to the heat balance. The net overall heat available raises the slag and metal temperature with time. The simulations suggest that the difference between metal and slag temperatures is usually small, except the peak decarburization period. During peak decarburization, the temperature difference between
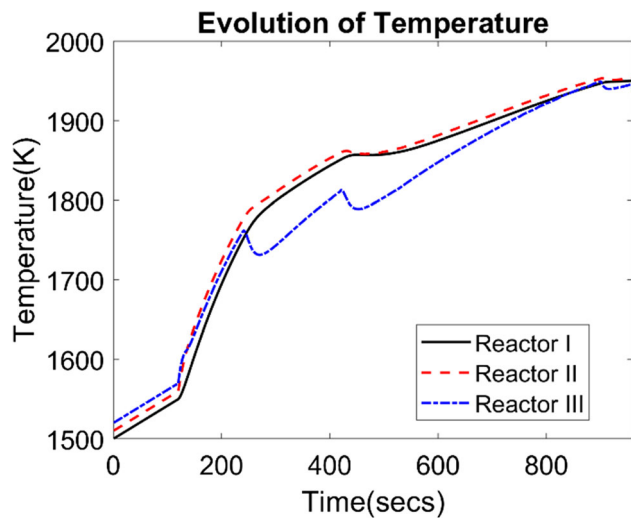
the slag and the metal is significant since rate of carbon oxidation is high and the amount of metal droplets *(that convey heat to the metal bath)* falling back to Reactor II is small. To oxidize carbon, enough oxygen must be supplied by dissociating iron oxide in the emulsion. So, the lowering of Reactor III temperature during mid-blow period can be attributed to this endothermic dissociation reaction. One can observe the jaggedness in the temperature variation of slag, which follows the pattern of lance height variation. On the other hand, the temperature in Reactors I and II varies smoothly as the reactions in the emulsion do not affect the temperature of these reactors directly, but only through the sensible heat of the falling droplets. The model predicts a nonlinear rise in temperature, which is in qualitative agreement with the operating trend in a typical BOF.[70,68]

VI. DISCUSSION

The model developed in course of the current work shows a fairly good agreement with plant trial data in terms of prediction of the evolution of metal composition with blowing time. It can be seen that maximum removal of silicon takes place during the initial couple of minutes when emulsion formation is insignificant, and the ejected droplets fly through the gas atmosphere. The interfacial concentration of silicon in equilibrium with the gas is found to be very small (~ 10^{-15}). The large difference in concentration of silicon between bulk and interface in the droplets drives the high rate of desiliconization. The predicted desiliconization profile agrees quite well with in-blow measurements showing near-total removal of dissolved silicon within 20 to 25 pct of the blow.[9,68,44] Manganese removal is also significant during this period but is less vigorous than that of silicon, in line with the thermodynamic driving force. The current model assumes that formation of SiO_2 and MnO at the gas/metal interface has minimal effect in

terms of blocking the reaction sites. As the flight time of droplets in the gas phase is very short, the assumption is justified.

The rate of generation of FeO in the impingement zone is nearly constant throughout the blowing period for fixed flow rate of oxygen, whereas the rate of consumption varies with the progress of the metalloid refining reactions. The rate of consumption is comparatively lower initially followed by a sudden rise in the mid-blow period and subsequently slowing down at the end-blow period. During the mid-blow period, droplet generation rate increases due to higher rate of transfer of momentum from oxygen jet at lower lance height. At the same time, the residence time of these droplets in the emulsion increases due to huge rate of generation of CO gas. Large slag/metal surface area from huge number of metal droplets in emulsion increases the rate of consumption of oxygen at the mid-blow period. With the progress of refining reactions, a point reaches when the oxygen demand exceeds the rate of supply of oxygen from the lance and the drop in FeO concentration profile can be attributed to this point. The low concentration of FeO in the slag prompts the reversion of phosphorus as well as manganese from the slag to the metal phase during the mid-blow. With eventual decrease in decarburization rate, FeO generation continues and allowing further removal of phosphorus and manganese from the metal. The current model does not consider bloating of the droplets due to internal nucleation of CO bubbles. Chen and Coley[71] investigated the bloating behavior of droplets due to retained CO bubbles while decarburizing in oxidizing slag. They proposed a modified classical nucleation theory by incorporating a parameter ψ that reduced the interfacial tension to a very low value, in order to match with the experimentally observed rate of CO generation. However, this parameter did not have any physical significance and further research remains necessary to quantify the extent of increase in slag/metal surface area due to bloating. The effect of bloating on dephosphorization reaction kinetics has been studied by Gu et al.[72] They have proposed that dephosphorization kinetics is enhanced due to bloating due to increase in interfacial area as well as stirring by CO bubbles. There is also possibility of further increase in interfacial area due to spontaneous emulsification of droplets in the oxidizing slag, which, according to Gaye and Riboud[73] as well as Spooner et al.,[74] resulted in higher rate of oxygen transfer through the slag–metal interface. Acknowledging the relatively weaker theoretical understanding in this context, the current authors have consciously stayed away from incorporating the increase in slag–metal interfacial area during reactions and its impact on the kinetics of phosphorus and manganese removal during the mid-blow period.

The authors believe that considering a linear rate of lime dissolution[75] was a reasonably good approximation for the initial and mid-blow periods. However, chance of significant deviation towards the end of the blow cannot be ruled out. Gradual reduction in the stirring intensity due to reduced rate of CO bubble formation and complete dissolution of lime before the end-blow state or the slag composition reaching CaO saturation are some of the likely reasons for variation of CaO-dissolution kinetics. The current model defines a single mass transfer coefficient in the slag phase throughout the blowing period. This can be improved further by considering the stirring introduced due to generation of CO bubbles from decarburization reaction at interface of each droplet. The transition from metal–gas reaction to metal–slag reaction was assumed to happen after approximately two minutes from start of refining, in this model. Further investigation is necessary to better understand the kinetics of reactions during the initial stage of refining in the BOF.

VII. CONCLUSION

The overall model was developed considering a linear profile of scrap and lime dissolution. Estimations of the evolution of temperature and composition were quite satisfactory. A new mechanism of reaction(s) occurring during the initial period, when the emulsion is yet to form, has been incorporated in the model. A new formulation for single-droplet reaction has been proposed for the droplet emulsion reaction by which faster silicon removal within first few minutes of the blow, carbon removal to 0.02 pct within 16 minutes, reversal of manganese and phosphorus, as well as subsequent removal to the slag have been predicted well. A key success of this model has been in simulating the reversion of manganese and phosphorus during the mid-blow period. The evolution of temperature has also been predicted as a function of blowing time. Further investigation is needed to fully incorporate the kinetics of the desiliconization as well as bloating of metal droplets during the refining process.

NOTATIONS

N_B	Blowing number (–)
ρ_g	Density of gas (kg/m^3)
ρ_M	Density of liquid metal (kg/m^3)
ρ_{slag}	Density of slag (kg/m^3)
u_g	Critical oxygen jet velocity (m/s)
u_0	Ejection velocity of metal droplets in gas phase from metal bath (m/s)
σ	Surface tension (N/m)

g	Gravitational constant (m/s^2)
R	Cumulative wt (in pct) retained on the sieve (pct)
d	Upper limit of class diameter in a given class (m)
d'	Characteristic diameter (m)
d_{limit}	Limiting diameter of the drop corresponding to R = 0.1 pct (m)
N	No of nozzles (–)
d_t	Throat diameter of nozzles (m)
x	Lance height (m)
p_0	Supply pressure of oxygen or nozzle exit pressure (Pa)
p_a	Ambient pressure (Pa)
θ	Angle of inclination of each nozzle relative to lance axis (deg)
θ_0	Angle of ejection of metal droplets in gas phase from metal bath (deg)
T	Temperature (K)
$X_{M_mO_n}, X^i_{M_mO_n}$	Mole fraction of species M_mO_n in bulk slag (M_mO_n = SiO_2, CaO, MgO) and at the slag metal interface (–)
$[\text{Pct M}]^i$, $[\text{Pct M}]^b$	Composition of metalloid M (M = C, O, Mn, Si, P) in metal phase at the interface and bulk phase, respectively (wt pct)
$[\text{Pct } M_mO_n]^i$, $[\text{Pct } M_mO_n]^b$	Composition of species M_mO_n (M_mO_n = SiO_2, FeO, P_2O_5) in slag phase at the interface and bulk phase, respectively (wt pct)
k^m_M	Mass transfer coefficient of metalloid M (= C, Si, Mn, P, O) in metal phase (m/s)
k_{slag}	Mass transfer coefficient in slag phase (m/s)
D_i	Mass transfer coefficient of metalloids i (i = C, Si, Mn, P, O) in metal phase (m^2/s)
t_{flight}	Time of flight of metal droplets in gas phase from bath (s)
$\gamma^b_{M_mO_n}$	Activity coefficient of species M_mO_n in slag (M_mO_n = SiO_2, FeO, P_2O_5, MnO) (–)
f^b_M	Henrian activity coefficient of metalloid M (M = C, O, Mn, Si, P) (–)
A	Surface area (gas/metal and slag/metal) (m^2)
N_O	No of moles of oxygen (moles)

REFERENCES

1. World Steel Association: *World Steel Association Report 2020*, 2020.
2. H.W. Meyer, W.F. Porter, G.C. Smith, and J. Szekely: *J. Met.*, 1968, pp. 35–42.
3. D.J. Min and R.J. Fruehan: *Metall. Mater. Trans. B*, 1992, vol. 23B, pp. 29–37.
4. C.L. Molloseau and R.J. Fruehan: *Metall. Mater. Trans. B Process Metall. Mater. Process. Sci.*, 2002, vol. 33B, pp. 335–44.
5. L.A. Baker, N.A. Warner, and A.E. Jenkins: *Trans. Metall. Soc.*, 1967, vol. 239, pp. 857–64.
6. S. Basu, A.K. Lahiri, and S. Seetharaman: *MetallMetall. Mater. Trans. B Process Metall. Mater. Process. Sci.*, 2007, vol. 38B, pp. 357–66.
7. S. Ohguchi, D.G.C. Robertson, B. Deo, P. Grieveson, and J.H.E. Jeffes: *Ironmak. Steelmak.*, 1984, vol. 11, pp. 202–13.
8. K. Gu, N. Dogan, and K.S. Coley: *Metall. Mater. Trans. B Process Metall. Mater. Process. Sci.*, 2017, vol. 48B, pp. 2343–53.
9. S. Basu, A.K. Lahiri, S. Seetharaman, and J. Halder: *ISIJ Int.*, 2007, vol. 47, pp. 766–8.
10. A.N. Assis: *Carnegie Mellon University*, 2014.
11. H. Sun: *ISIJ Int.*, 2006, vol. 46, pp. 1560–9.
12. M.Z. Benk and G. Kaptay: *Mater. Sci. Forum*, 2003, vols. 414–415, pp. 365–70.
13. R.K. Jain: *Indian Institute of Science*, India, 1974.
14. B. Tang, W. Zhang, X. Wang, G. Sun, Y. Yu, H. Zongshu, and A. Yu: in *Proceedings of the 8th Pacific Rim International Congress on Advanced Materials and Processing*. Springer, Cham, 2013.
15. B. Deo, P. Ranjan, and A. Kumar: *Steel Res.*, 1987, vol. 58, pp. 427–31.
16. W. van der Knoop, B. Deo, A.B. Snoeijer, G. van Unen, and R. Boom: *4th Int. Conf. Molten Slags Fluxes*, 1992, pp. 302–7.
17. C. Kattenbelt and B. Roffel: *Metall. Mater. Trans. B*, 2008, vol. 39B, pp. 764–9.
18. F. Pahlevani, S. Kitamura, H. Shibata, and N. Maruoka: *ISIJ Int.*, 2010, vol. 50, pp. 822–9.
19. A.K. Shukla, B. Deo, S. Millman, B. Snoeijer, A. Overbosch, and A Kapilashrami: *Steel Res. Int.*, 2010, vol. 81, pp. 940–48.
20. N. Dogan, G.A. Brooks, and M.A. Rhamdhani: *ISIJ Int.*, 2011, vol. 51, pp. 1093–101.
21. N. Dogan, G.A. Brooks, and M.A. Rhamdhani: *ISIJ Int.*, 2011, vol. 51, pp. 1086–92.
22. N. Dogan, G.A. Brooks, and M.A. Rhamdhani: *ISIJ Int.*, 2011, vol. 51, pp. 1102–9.
23. E. Graveland-Gisolf, P. Mink, A. Overbosch, R. Boom, G. De Gendt, and B. Deo: *Steel Res.*, 2003, vol. 74, pp. 125–30.
24. Y. Lytvynyuk, J. Schenk, M. Hiebler, and A. Sormann: *Steel Res. Int.*, 2014, vol. 85, pp. 537–43.
25. Y. Lytvynyuk, J. Schenk, M. Hiebler, and A. Sormann: *Steel Res. Int.*, 2014, vol. 85, pp. 544–63.
26. B.K. Rout, G.A. Brooks, Z. Li, and M.A. Rhamdhani: *AISTech - Iron Steel Technol. Conf. Proc.*, 2016, vol. 1, pp. 1019–26.
27. B.K. Rout, G.A. Brooks, Z. Li, and M.A. Rhamdhani: *AISTech - Iron Steel Technol. Conf. Proc.*, 2015, vol. 3, pp. 3225–37.
28. B.K. Rout, G. Brooks, M. Akbar Rhamdhani, Z. Li, F.N.H. Schrama, and W. van de rKnoop: *Metall. Mater. Trans. B Process Metall. Mater. Process. Sci.*, 2018, vol. 49, pp. 2191–208.
29. B.K. Rout, G. Brooks, M.A. Rhamdhani, Z. Li, F.N.H. Schrama, and A. Overbosch: *Metall. Mater. Trans. B*, 2018, vol. 49B, pp. 1022–33.
30. A. Kruskopf and V.V. Visuri: *Metall. Mater. Trans. B Process Metall. Mater. Process. Sci.*, 2017, vol. 48, pp. 3281–300.

31. A. Kadrolkar and N. Dogan: *Metall. Mater. Trans. B Process Metall. Mater. Process. Sci.*, 2019, vol. 50, pp. 2912–29.
32. A. Kadrolkar and N. Dogan: *Metals (Basel)*, 2019, vol. 9, p. 309.
33. D. Dering, C. Swartz, and N. Dogan: *Processes*, 2020, vol. 8, pp. 1–23.
34. M. Han and Y. Zhao: *Expert Syst. Appl.*, 2011, vol. 38, pp. 14786–98.
35. L.F. Xu, W. Li, M. Zhang, S.X. Xu, and J. Li: *Optik (Stuttg)*, 2011, vol. 122, pp. 594–98.
36. F. He and L. Zhang: *J. Process Control*, 2018, vol. 66, pp. 51–8.
37. J. Kacur, M. Laciak, P. Flegner, J. Terpak, M. Durdan, and G. Trefa: *Proc. 2019 20th Int. Carpathian Control Conf. ICCC 2019*, DOI:10.1109/CarpathianCC.2019.8765956.
38. A. Rahnama, Z. Li, and S. Sridhar: *Processes*, 2020, vol. 8, pp. 169–177.
39. S. Ghosh, N.B. Ballal, and N.N. Viswanathan: *Miner. Process. Extr. Metall. Trans. Inst. Min. Metall.*, 2019, vol. 128, pp. 17–33.
40. L DeVos, I Bellemans, C Vercruyssen, and K Verbeken: *Metall. Mater. Trans. B Process Metall. Mater. Process. Sci.*, 2019, vol. 50, pp. 2647–66.
41. R. Sarkar, P. Gupta, S. Basu, and N.B. Ballal: *Metall. Mater. Trans. B*, 2015, vol. 46B, pp. 961–76.
42. J. Biswas: *Indian Institute of Technology Bombay*, 2015.
43. S. Ghosh: *Indian Institute of Technology Bombay*, 2014.
44. C. Cicutti, M. Valdez, T. Perez, J. Petroni, A. Gomez, R. Donayo, and L. Ferro: in *6th International Conference on Molten Slags, Fluxes and Salts, Stockholm- Helsinki, 2000,Paper 367*, 2000, pp. 1–9.
45. C. Cicutti, M. Valdez, T. Pérez, R. Donayo, and J. Petroni: *Lat. Am. Appl. Res.*, 2002, vol. 32, pp. 237–40.
46. G. Turner and S. Jahanshahi: *Trans. Iron Steel Inst. Japan*, 1987, vol. 27, pp. 734–39.
47. Q.L. He and N. Standish: *ISIJ Int.*, 1990, vol. 30, pp. 356–61.
48. Q. He: *The University of Wollongong*, 1991.
49. Subagyo, G.A. Brooks, K.S. Coley, and G.A. Irons: *ISIJ Int.*, 2003, vol. 43, pp. 983–89.
50. Q.L. He and N. Standish: *ISIJ Int.*, 1990, vol. 30, pp. 305–309.
51. SC Koria and KW Lange: *Metall. Trans. B*, 1984, vol. 15B, pp. 109–16.
52. P. Rosin, E. Rammler, and W. Intelmann: *VDI Zeitschrift*, 1932, vol. 76, pp. 433–37.
53. Subagyo and G.A. Brooks: *ISIJ Int.*, 2002, vol. 42, pp. 1182–84.
54. B. Deo, A. Karamcheti, A. Paul, P. Singh, and R.P. Chhabra: *ISIJ Int.*, 1996, vol. 36, pp. 658–66.
55. G.K. Sigworth and J.F. Elliott: *Met. Sci.*, 1974, vol. 8, pp. 298–310.
56. M. Allibert, R. Parra, C. Saint-Jours, and M. Tmar: in *Slag Atlas*, VDEh, ed., 2nd edn., 1995, p. 244.
57. E.T. Turkdogan and R.J. Fruehan: in *The Making, Shaping and Treating of Steel, Steelmaking and Refining Volume, 11th ed., RJ Fruehan, ed., AISE Steel Foundation, Pittsburgh*, vol. 11, 1998, p. 88.
58. S. Basu, A.K. Lahiri, and S. Seetharaman: *Metall. Mater. Trans. B Process Metall. Mater. Process. Sci.*, 2008, vol. 39, pp. 447–56.
59. S. Basu, A.K. Lahiri, and S. Seetharaman: *ISIJ Int.*, 2007, vol. 47, pp. 1236–38.
60. R. Higbie: *Trans. Am. Inst. Chem. Eng.*, 1935, vol. 31, pp. 365–389.
61. K. Koch, W. Fix, and P. Valentin: *Arch Eisenhuettenwes*, 1978, vol. 49, pp. 163–66.
62. Y.E. Lee and L. Kolbeinsen: *ISIJ Int.*, 2007, vol. 47, pp. 764–65.
63. Y. Chung and A.W. Cramb: *Metall. Mater. Trans. B*, 2000, vol. 31B, pp. 957–71.
64. D. Goldberg and G.R. Belton: *Met. Trans*, 1974, vol. 5, pp. 1643–48.
65. F.P. Calderon, N. Sano, and Y. Matsushita: *Metall. Mater. Trans. B*, 1971, vol. 2B, pp. 3325–32.
66. Q. He: *The University of Wollongong*, 1990.
67. L. Cao, Q. Liu, J. Sun, W. Lin, and X. Feng: *JOM*, 2019, vol. 71, pp. 754–63.
68. M. Millman, A. Kapilashrami, M. Bramming, and D. Malmberg: *Imphos: Improving Phosphorus Refining*, 2011.
69. M. Swinnerton: *University of Wollongong*, 2005.
70. S. Asai and I. Muchi: *Trans. Iron Steel Inst. Japan*, 1970, vol. 10, pp. 250–63.
71. E. Chen and K.S. Coley: *Ironmak. Steelmak.*, 2010, vol. 37, pp. 541–45.
72. K. Gu: McMaster University, 2017.
73. H. Gaye and P.V. Riboud: *Metall. Trans. B*, 1977, vol. 8B, pp. 409–15.
74. A.N. Assis, J. Warnett, S. Spooner, R.J. Fruehan, M.A. Williams, and S. Sridhar: *Metall. Mater. Trans. B Process Metall. Mater. Process. Sci.*, 2015, vol. 46, pp. 568–76.
75. M. Matsushima, S. Yadoomaru, K. Mori, and Y. Kawai: *Trans. Iron Steel Inst. Japan*, 1977, vol. 17, pp. 442–49.